All-optical switching of liquid crystals at terahertz frequencies enabled by metamaterials

BEN BEDDOES,[1,*] ![iD] ELENI PERIVOLARI,[1,2]
MALGOSIA KACZMAREK,[1] VASILIS APOSTOLOPOULOS,[1] ![iD]
AND VASSILI A. FEDOTOV[3]

[1] *Physics and Astronomy, University of Southampton, Highfield, SO17 1BJ, UK*
[2] *EMPA Swiss Federal Laboratories for Material Science and Technology, Ueberlandstrasse 129, 8600 Dübendorf, Switzerland*
[3] *Optoelectronics Research Centre & Centre for Photonic Metamaterials, University of Southampton, Highfield, SO17 1BJ, UK*
*B.Beddoes@soton.ac.uk

Abstract: Nematic liquid crystals integrated with metallic resonators (metamaterials) are intriguing hybrid systems, which not only offer added optical functionalities, but also promote strong light-matter interactions. In this report, we show with an analytical model that the electric field generated by a conventional oscillator-based terahertz time domain spectrometer is strong enough to induce partial, all-optical switching of nematic liquid crystals in such hybrid systems. Our analysis provides a robust theoretical footing for the mechanism of all-optical nonlinearity of liquid crystals, which was recently hypothesised to explain an anomalous resonance frequency shift in liquid crystal-loaded terahertz metamaterials. The integration of metallic resonators with nematic liquid crystals offers a robust approach to explore optical nonlinearity within such hybrid material systems in the terahertz range; paves the way towards increased efficiency of existing devices; and broadens the range of applications of liquid crystals in the terahertz frequency range.

1. Introduction

Terahertz (THz) technologies have shown significant potential in several important application areas including: non-disruptive drugs sensing [1,2], security [3–5], medicine and life sciences [6] and next-generation short-range wireless systems operating at higher data transfer rates than currently available [7]. Yet, research in this field is still primarily focused on finding ways to both control and manipulate THz radiation effectively [8–11]. A particular focus is on the development of tuneable, compact and cheap devices such as modulators [12,13] and phase shifters [14]. Liquid crystals (LCs) could offer a viable solution being already at the core of many technologies across most of the electromagnetic spectrum, such as: smart displays [15,16], smart windows [17,18], flat optics [19–22], and flexible electronics [23–25]. However, to operate efficiently in the THz spectral domain, LC-based optical components must be several hundred microns (or more) thick. This is due to the relatively low birefringence of available LC materials and the long wavelength of THz radiation. Furthermore, LC-based devices are typically controlled by externally applied electric fields, which necessitates the use of transparent electrodes [26,27] not readily available in all regions of the spectrum, especially in THz [28].

The efficiency of LC-based devices in the THz regime can be substantially improved by the inclusion of metallic planar metamaterials (MMs). Such MMs are thin, metal films patterned on a sub-wavelength scale, enabling dramatic enhancement of diffraction-free light-matter interactions, while maintaining a small device footprint [13,29]. Recently, LC optical devices based on MM concepts have shown considerable potential as active THz beam deflectors and spin-state

converters for use in wireless communication applications [30,31]. However, while there has been significant advancements in improving the resonator films and developing new alignment and electrode layers [32,33], the current operation of these devices still requires external control through the application of static and quasi-static fields or temperature [13,29,34–41].

In our recent work we reported the first indication of LC all-optical switching in THz hybrid MM devices [42]. We speculated that an observed frequency shift, larger than predicted by a rigorous numerical model, was a result of a local in-plane re-orientation of LC molecules induced by incident THz fields, which underwent resonant amplification and sub-wavelength concentration facilitated by the fabric of MMs. Here, we provide a comprehensive theoretical description and analysis of the proposed mechanism based on an analytical model of in-plane switching (IPS). While the latter was originally developed for conventional electro-optical LC cells, we show how the IPS model can be extended and adapted to describe localised LC switching induced optically in a hybrid MM device. The novel approach developed here enabled us to conclude that engaging orientational optical nonlinearity of LCs at typical THz time domain spectrometer (TDS) intensities is achievable with metallic MMs.

2. Experimental demonstration of optical switching

For the sake of completeness and convenience to the reader, in this section we provide a brief account of our first experimental indication of all-optical switching in LC-loaded THz MMs [42]. This study involved the characterisation of the transmission spectra of 20 μm thick LC optical cells hybridised with metallic resonator films in positive and negative MM configurations and for different LC alignment directions. This was achieved using a conventional oscillator based THz-TDS setup in the 0.1–1.4 THz range of frequencies. The hybrid cells were filled with the highly birefringent nematic LC1825. Prior to cell assembly, a thin layer of polyimide was spin-coated over both the top and bottom surfaces of the cell, then mechanically rubbed to ensure uniform planar alignment of the LCs in the absence of external stimuli. For the configuration illustrated in Fig. 1(a), where LC alignment was set parallel to the straight edges of the metamolecules, the measured spectrum shown with a black dashed line in Fig. 2(a) appeared red-shifted with respect to the spectrum simulated for planar LC configuration (blue solid line). The experimental results also displayed a smaller variation of transmission at the resonance. It was speculated that this surprising discrepancy was the result of optically-induced local distortions of the initially planar alignment of the LCs near the corners of the metamolecules ('hotspots'), where the re-orientation of LC molecules was driven by the resonantly amplified near field of the MMs (see Fig. 2(b)).
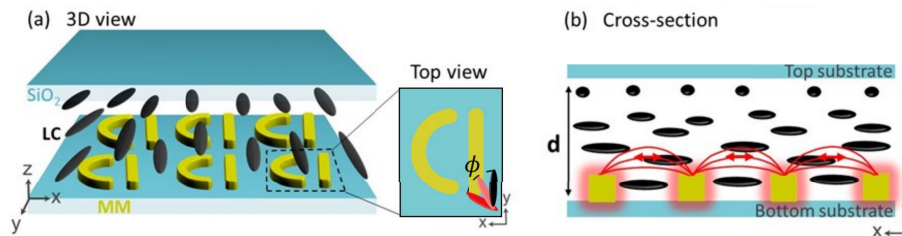

Fig. 1. (a) An artistic impression of a homogeneously aligned planar LC cell integrated with an array of D-shaped metallic resonators (metamaterial). Inset shows schematically changes in the orientation of an LC molecule near a D-shaped resonator (and the associated twist angle, ϕ), driven by the near field. (b) Schematic representation of in-plane LC switching near the metamaterial induced by its resonantly enhanced near field (red arrows) in a homogeneously aligned hybrid LC cell.
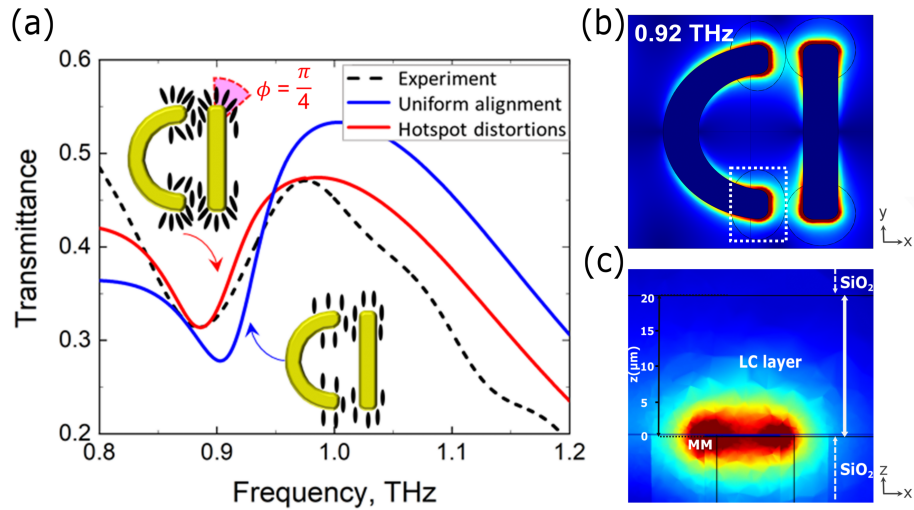
Fig. 2. (a) Transmission spectra of LC-loaded MM measured experimentally (black dash line) and modelled numerically in the cases when LC alignment is planar and uniform everywhere (blue solid curve) and distorted locally within 'hotspots' (red solid curve). Insets illustrate schematically the local alignment of LC molecules assumed in the two cases. Angle ϕ describes the twist deformation of LC in the 'hotspots' and has the maximum value of $\frac{\pi}{4}$. (b) Field map shows the variation of electric field induced in the plane of a metamolecule (*xy*-plane) at the resonance frequency of 0.92 THz. Electric field is strongest near the corners and in the gaps of the metamolecule. (c) Field map shows the variation of the in-plane component of electric field induced in *xz*-plane near the corner of the metamolecule (marked by white rectangle in panel (b)).

To this end, our initial numerical model (which informed the design of the hybrid MM device) was modified to include the change in the refractive index of the LCs near the corners and in the gaps of D-shaped metallic resonators that would result from the re-orientation of LC molecules along the field lines. However, this would only occur when the direction of the local field deviated from the initial LC alignment by no more than $\pi/4$ (see inset to Fig. 2(a)). For other directions, (i.e., from $\pi/4$ to $\pi/2$) the local field was deemed too weak to ensure the complete re-orientation of LC molecules along its field lines. The transmission spectrum of the MM calculated using the modified numerical model is plotted in Fig. 2(a) with a red solid line and shows a good spectral overlap with the experimental data, thus, rendering plausible our hypothesis that the deformation of planar LC alignment, ϕ, of up to $\pi/4$ was induced optically within the 'hotspots'. From the numerical calculations we also found that the overall local-field enhancement attainable with the MM film was likely to exceed 200 [42], which suggested that in our case the orientational optical nonlinearity of LC might be engaged even with a low-power THz-TDS. In this work, we build on our preliminary calculations to validate the above hypothesis. The analytical model proposed here is based on a novel use and the adaptation of the IPS model for LC switching in metamaterials and plasmonic structures.

3. Analytical model of LC optical switching

To estimate the strength of the THz field required to switch LCs in such hybrid cells we used a mathematical model previously developed for the analysis of the IPS of nematic LCs in conventional electro-optical cells [43]. Briefly, in the IPS model the electric field that re-orients

LC molecules is produced by interdigital electrodes, which have an infinite length and are all arranged on the same plane (e.g., the surface of a substrate), forming two interlocking combs. It is assumed that every pair of neighbouring electrodes acts like a capacitor so that the electric field is homogeneous and aligned parallel to the substrate. In the OFF state, the LC molecules are oriented along the electrodes (see Fig. 3(a)). In the ON state, the electric field of the electrodes forces the LC molecules to orient along the field lines, i.e., orthogonal to the electrodes. Thus, IPS corresponds to $\pi/2$ "in-plane" twist deformation of the LCs (see Fig. 3(a)) [44,45]. Similarly, we assume that in our case the electric field induced at the corners of the metamolecules, upon their illumination with a THz beam (ON state), drives the re-orientation of LC molecules within the "hotspots". This occurs in the plane of the MM, towards the direction of the field lines (see Fig. 1(b)). What makes our case principally different from the conventional IPS model is that the electric field acting on the LCs does not extend all the way across the cell, but is rather confined to a distance of a few microns above the MMs. More specifically, given that the local field decays exponentially within the hotspots, which is supported by the result of our simulation (see Fig. 2(c)), the spatial extent of the electric field is capped by $z_c = 2.9$ μm, as given by exp(-1) falloff of the electric field strength. Thus, we use the IPS model approach locally, in close vicinity to the metamolecules, where this "local" electric field is further assumed to be uniform and aligned parallel to the substrate. As part of our investigation, we also compared the strengths of the z-component and in-plane component of the local electric field within the active regions and found the former to be a factor 3 weaker than the latter. Hence, the LC re-orientation occurs predominantly in 2D. In any case, our analytical model underestimates the strength of the effect, since admitting the orientation of LC molecules in 3D will make the local change of the refractive index of LC only larger. Another principle difference with the conventional IPS model is that the twist deformation of the LC, ϕ, in the areas featuring complete in-plane switching does not exceed $\pi/4$, as illustrated in Fig. 3(b). This fact was established earlier in [42] and, as we will show below, it lifts the restriction on the minimal strength of the electric field (i.e., voltage threshold) that can drive in-plane re-orientation of LC molecules and the resulting orientational optical nonlinearity of LCs in the THz regime.
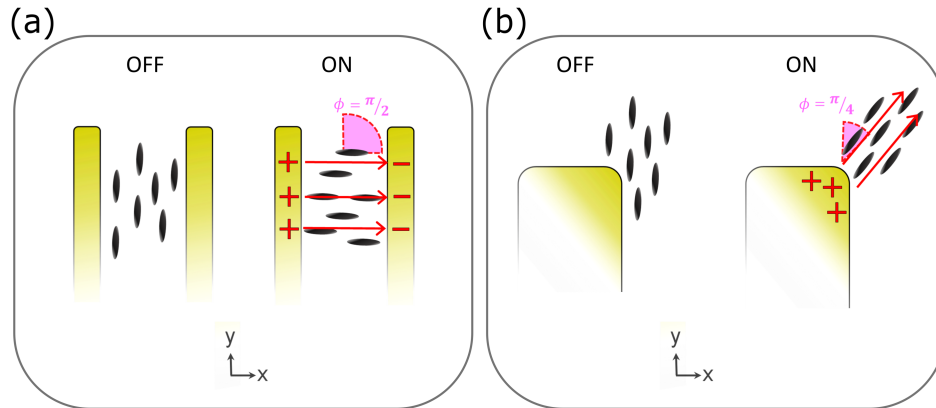

Fig. 3. (a) Schematically shown conventional in-plane switching mode of an LC cell (b) Schematically shown in-plane switching driven by the near field of a metamolecule, which models the re-alignment of LC in the area of the 'hotspot' where the initial misalignment between LC director and local field reaches $\pi/4$.

Following [43], we start with the free energy functional $F(\phi)$ of the twist deformation for the layer of LC subjected to the local electric field ($0 \le z \le z_c$), which has the form

$$F(\phi) = \frac{1}{2} \int_0^{z_c} \left(K_2 \left(\frac{d\phi}{dz} \right)^2 - \epsilon_0 \left| \Delta \epsilon \right| E^2 \sin^2 \phi \right) dz \tag{1}$$

where K_2 is the elastic constant of the twist deformation, ϕ is the twist angle in the xy-plane, $\Delta\epsilon$ denotes the dielectric anisotropy of the LCs, and E is the strength of the in-plane component of the local electric field. To further simplify the analysis, E is taken to be constant with the value given by the strength of local field averaged across $0 \le z \le z_c$. To minimise the functional Eq. (1), ϕ must satisfy the following Euler-Lagrange equation.

$$K_2 \frac{d^2\phi}{dz^2} + \epsilon_0 \left| \Delta \epsilon \right| E^2 \sin \phi \cos \phi = 0 \tag{2}$$

In the IPS model ϕ is defined as the angle between LC director and the direction orthogonal to the electric field lines and, hence, due to the initially planar alignment, LCs in the hotspots appear twisted with respect to the local field lines with ϕ being equal to or exceeding $\pi/4$ [42]. Thus, for those sectors of the hotspots that permit the largest optically-induced twist deformation the following substitution can be made: $\phi = \phi + \pi/4$, where ϕ now describes the deformation relative to the initial twist. As a result, Eq. (2) transforms into

$$K_2 \frac{d^2\phi}{dz^2} + \frac{\epsilon_0 \left| \Delta \epsilon \right| E^2}{2} \cos 2\phi = 0 \tag{3}$$

We proceed by solving Eq. (3) first under the assumption that the relative twist deformation is small, i.e., $\phi \to 0$. To find the solution we apply the following boundary conditions: $\phi = 0$ at $z = 0$ (corresponds to strong LC anchoring imposed on the MM side of the cell by rubbed polyimide) and $\frac{d\phi(z)}{dz} = 0$ at $z = z_c$, which stems from the transversality condition and effectively defines z_c as a "free" boundary. The inclusion of this 'free' boundary condition eliminates any restriction attributed to anchoring at hard boundaries. This enables the wider implementation of our model to different cell thicknesses, allowing for further exploration beyond the specific system addressed in this paper. In this case we arrive at the following solution

$$\phi(z) = \frac{\epsilon_0 \left| \Delta \epsilon \right| E^2}{4K_2} (2z_c - z)z \tag{4}$$

Evidently, Eq. (4) yields a non-zero ϕ for any $E \ge 0$, which indicates that the in-plane re-orientation of LC molecules within the hotspots starts with no threshold on the strength of the local electric field. This is in stark contrast to the conventional IPS model, which manifests itself as a Fréedericksz transition and typically cannot be engaged with electric fields weaker than 1.05 V/cm [43].

Next, we aim to find an analytical solution of Eq. (3), which will be valid in the limit of large relative twist angles, i.e., $\phi \to \pi/4$. To this end we linearise Eq. (3) by replacing $\cos 2\phi$ in the second term with its linear approximation at $\phi = \pi/4$. Here we have chosen the linear function that is tangential to $\cos 2\phi$ at $\phi = \pi/4$ (black dashed line Fig. 4(a)).

To this end, we use the approximation

$$\cos 2\phi \approx \pi/2 - 2\phi \tag{5}$$

which turns the initially nonlinear differential Eq. (3) into

$$K_2 \frac{d^2\phi}{dz^2} - \epsilon_0 \left| \Delta \epsilon \right| E^2 \phi + \epsilon_0 \left| \Delta \epsilon \right| E^2 \frac{\pi}{4} = 0 \tag{6}$$
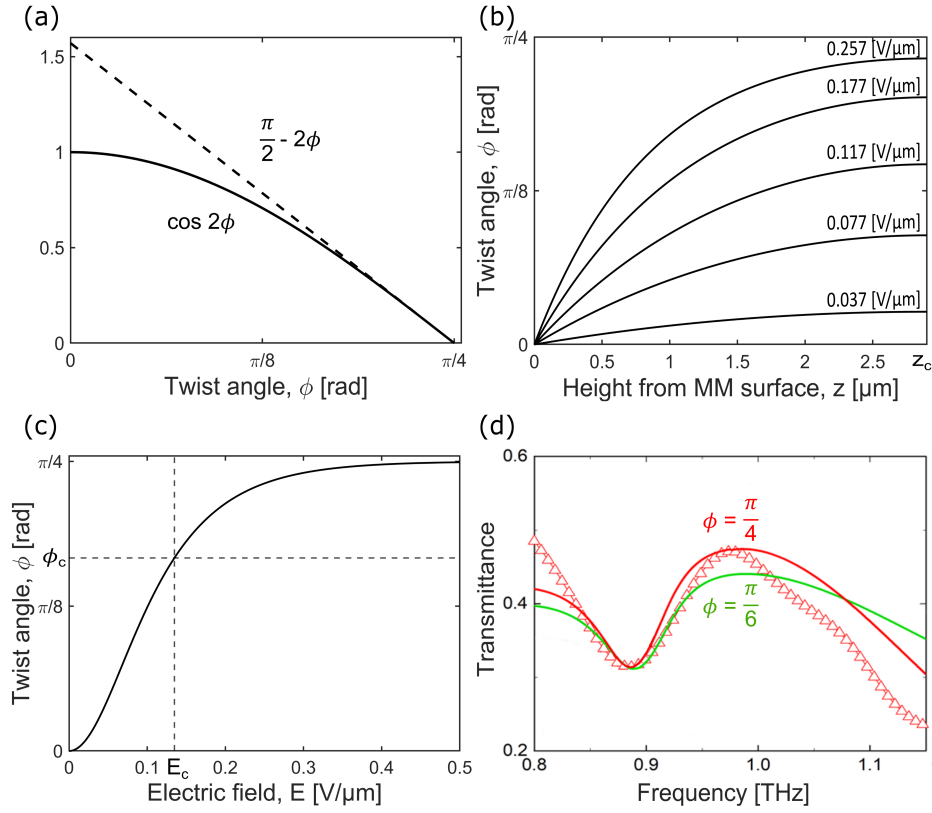
Fig. 4. (a) The linear approximation of $\cos 2\phi$ (solid line) approximated using $\frac{\pi}{2} - 2\phi$ (dashed line). (b) The change of twist angle, ϕ, within LC layer ($0 \geq z \geq z_c$), for different E-field values using the $\frac{\pi}{2} - 2\phi$ approximation. (c) The maximal twist angle, ϕ, achieved at $z = z_c$ as a function of the local electric-field strength, E. (d) Simulated results of the transmission spectra for hybrid LC cells at different angular limits of re-orientation around MM 'hotspots' (solid lines), with experimental results (open triangles).

Equation (6) can now be solved analytically and its solution is given by

$$\phi(z, E) = \frac{\pi}{4} + k_1 \exp\left(-\sqrt{\frac{\epsilon_0 |\Delta\epsilon|}{K_2}} Ez\right) + k_2 \exp\left(\sqrt{\frac{\epsilon_0 |\Delta\epsilon|}{K_2}} Ez\right) \tag{7}$$

To determine k_1 and k_2, we use the same boundary conditions as above, namely $\phi(0) = \frac{d\phi(z_c)}{dz} = 0$. The derived expressions for k_1 and k_2 are

$$k_1 = -\left(\frac{\pi}{4} + k_2\right) \tag{8}$$

$$k_2 = -\frac{\pi \exp\left(-\sqrt{\frac{\epsilon_0 |\Delta\epsilon|}{K_2}} Ez_c\right)}{8\left(\cosh\left(\sqrt{\frac{\epsilon_0 |\Delta\epsilon|}{K_2}} Ez_c\right)\right)} \tag{9}$$

The constants in Eq. (7), (8) and (9) for LC1825 are taken from [46] (see Table 1).

Table 1. Specifications of LC1825 [46]

Constants	Values
ϵ_0	8.85×10^{-12} [N/V^2]
$\Delta\epsilon$	17
K_2	7.4×10^{-12} [N]

4. Discussion

Figure 4(b) shows how the twist angle varies within a 2.9 μm layer of LC around the MM, as calculated using Eq. (7) for different values of the local electric-field strength. Evidently, the twist deformation increases monotonously away from the MM and saturates on approaching z_c. Note that while in-plane switching in our case features no voltage threshold, it formally remains incomplete since the analytical solution approaches $\pi/4$ asymptotically. This is best illustrated by Fig. 4(c), where we plot the maximal twist angle (achieved at $z = z_c$) as a function of the local electric-field strength. Such behavior is underpinned by the dependence of the electrically induced LC torque on the twist angle. The torque in our case is proportional to $\cos 2\phi$ and, therefore, decreases with increasing ϕ, vanishing completely for LC molecules aligned parallel to the electric field (i.e., when $\phi = \pi/4$). In practice, however, the switching of LCs within the hotspots does not have to be complete, as the dielectric permittivity of LC "sensed" there by the local electric field is proportional to $\cos \Delta\phi$, where $\Delta\phi = \pi/4 - \phi$. If $\Delta\phi << 1$ the deviation of dielectric permittivity from the maximum value will be proportional to $\Delta\phi^2$ and, hence, appear insignificant.

   Since the solution Eq. (7) is valid for $\phi \rightarrow \pi/4$, where the dependence on the local-field strength resembles a saturating exponential function (Fig. 4(c)), we take $\Delta\phi = \pi/4$. It corresponds to a twist angle of $\pi/6$, which we regard as the "characteristic" twist angle, ϕ_c. It defines $[0, \pi/6]$ as the range of LC twist deformations beyond which a significant change in the optical response of LC-loaded MM no longer occur, as also confirmed by our rigorous numerical modeling (see Fig. 4(d)). Hence, the characteristic twist angle can be used to determine the strength of local electric field, E_c, which would yield the level of optical switching comparable to that observed in the experiment [42]. Applying ϕ_c to the dependence plotted in Fig. 4(c) gives $E_c \approx 0.13$ V/μm.

   In the final part of our analysis we compare the typical strength of electric fields generated by a THz-TDS system with the strength of incident electric field required to seed the observed nonlinearity. To estimate the latter, we recall that local electric field decays exponentially away from the surface of the MM with e^{-1} falloff at 2.9 μm, while E_c in our analysis corresponds to the average value of the local-field strength. Hence, the electric field produced in the plane of the MM is a factor of 3 stronger than E_c. Since the field-enhancement factor characteristic of D-shaped metamolecules exceeds 200 [42], the required strength of electric field in an incident terahertz beam can be less than $3E_c/200 \approx 20$ V/cm. Given that in conventional THz-TDS setups the electric field peered by THz detectors has the strength in the range from 10 to 100 V/cm [47], we conclude that the orientational optical nonlinearity of LCs can be readily engaged at THz frequencies with the help of purposely designed metallic MMs (at least, at the modest level observed in [42]). Also, we envisage that further optimisation of MM designs and the use of stronger sources of THz radiation will allow one to maximise the extent of LC all-optical switching in hybrid cells by enabling complete re-orientation of LC molecules even in those areas of the hotspots, where the initial misalignment between LC director and local field exceeds $\pi/4$. Among potential candidates for the THz sources that would be required, we have identified quantum cascade laser systems, which can achieve powers on the order of microwatts and above [48].

5. Conclusion

In this work, we analysed the nonlinear optical response of a liquid crystal cell hybridised with a metallic metamaterial film and, in particular, a prominent shift of the metamaterial resonance frequency that can be observed using a conventional oscillator-based terahertz time domain spectrometer. We show that a local field enhancement exceeding a factor of 200 characteristic of the metamaterial film allows engagement of nonlinear effects, despite the relatively low intensity radiation used. Indeed, an analytical approach based on the adapted and tailored in-plane switching model of a conventional liquid crystal cell reveals that the re-orientation of liquid crystals near the metamaterial is a thresholdless process. Furthermore, an incident terahertz electric field of as low as $\approx 20V/cm$ is strong enough to ensure the degree of all-optical liquid crystal switching observed in the experiment. Our novel approach paves a way towards systematic quantitative investigation of nonlinear optical effects in metamaterial-enhanced liquid crystal devices using conventional THz-TDS systems, with prospects for the development of low-power terahertz all-optical switches, spatial light modulators and image processors.

Disclosures. The authors declare no conflicts of interest.

Data availability. Data underlying the results presented in this paper are available from the University of Southampton repository at [49].

References

1. J. Y. Lu, L. J. Chen, T. F. Kao, H. H. Chang, H. W. Chen, A. S. Liu, Y. C. Chen, R. B. Wu, W. S. Liu, J. I. Chyi, and C. K. Sun, "Terahertz microchip for illicit drug detection," IEEE Photonics Technol. Lett. **18**(21), 2254–2256 (2006).
2. S. Al Tahhan and H. Aljobouri, "Sensing of illegal drugs by using photonic crystal fiber in terahertz regime," *J. Opt. Commun.* **-1**, (2020).
3. E. Mavrona, U. Chodorow, M. E. Barnes, J. Parka, N. Palka, S. Saitzek, J. F. Blach, V. Apostolopoulos, and M. Kaczmarek, "Refractive indices and birefringence of hybrid liquid crystal - nanoparticles composite materials in the terahertz region," AIP Adv. **5**(7), 077143 (2015).
4. B. Ning, Z. Chen, W. Chen, and L. Li, "Improving security of thz communication with intelligent reflecting surface," *2019 IEEE Globecom Workshops, GC Wkshps 2019* - Proceedings (2019).
5. J. F. Federici, B. Schulkin, F. Huang, D. Gary, R. Barat, F. Oliveira, and D. Zimdars, "Thz imaging and sensing for security applications - explosives, weapons and drugs," Semicond. Sci. Technol. **20**(7), S266–S280 (2005).
6. P. Sharma, C. Liu, C. Ming, X. Wang, R. M. Woodward, B. E. Cole, V. P. Wallace, R. J. Pye, D. D. Arnone, E. H. Linfield, and M. Pepper, "Terahertz pulse imaging in reflection geometry of human skin cancer and skin tissue," Phys. Med. Biol. **47**(21), 3853–3863 (2002).
7. K. KrishneGowda, P. Rodriguez-Vazquez, L. Lopacinski, U. R. Pfeiffer, E. Grass, and R. Kraemer, "Thz transmission experiments - a data rate of 80 gbps was demonstrated using kasami codes," in *2021 IEEE International Conference on Microwaves, Antennas, Communications and Electronic Systems (COMCAS)*, (2021), pp. 163–168.
8. L. D. Sio, G. Klein, S. Serak, N. Tabiryan, A. Cunningham, C. M. Tone, F. Ciuchi, T. Bürgi, C. Umeton, and T. Bunning, "All-optical control of localized plasmonic resonance realized by photoalignment of liquid crystals," J. Mater. Chem. C **1**(45), 7483–7487 (2013).
9. H.-K. Lee, A. Kanazawa, T. Shiono, T. Ikeda, T. Fujisawa, M. Aizawa, and B. Lee, "All-optically controllable polymer liquid crystal composite films containing the azobenzene liquid crystal," Chem. Mater. **10**(5), 1402–1407 (1998).
10. E. Perivolari, J. R. Gill, N. Podoliak, V. Apostolopoulos, T. J. Sluckin, G. D'Alessandro, and M. Kaczmarek, "Optically controlled bistable waveplates," J. Mol. Liq. **267**, 484–489 (2018).
11. L. D. Sio, E. Ouskova, P. Lloyd, R. Vergara, N. Tabiryan, and T. J. Bunning, "Light-addressable liquid crystal polymer dispersed liquid crystal," Opt. Mater. Express **7**(5), 1581 (2017).
12. C. M. Watts, D. Shrekenhamer, J. Montoya, G. Lipworth, J. Hunt, T. Sleasman, S. Krishna, D. R. Smith, and W. J. Padilla, "Terahertz compressive imaging with metamaterial spatial light modulators," Nat. Photonics **8**(8), 605–609 (2014).
13. O. Buchnev, N. Podoliak, K. Kaltenecker, M. Walther, and V. A. Fedotov, "Metasurface-based optical liquid crystal cell as an ultrathin spatial phase modulator for thz applications," ACS Photonics **7**(11), 3199–3206 (2020).
14. P. Weis, J. L. Garcia-Pomar, M. Höh, B. Reinhard, A. Brodyanski, and M. Rahm, "Spectrally wide-band terahertz wave modulator based on optically tuned graphene," ACS Nano **6**(10), 9118–9124 (2012).
15. C. C. Li, H. Y. Tseng, C. W. Chen, C. T. Wang, H. C. Jau, Y. C. Wu, W. H. Hsu, and T. H. Lin, "Versatile energy-saving smart glass based on tristable cholesteric liquid crystals," ACS Appl. Energy Mater. **3**(8), 7601–7609 (2020).
16. J. R. Talukder, H.-Y. Lin, and S.-T. Wu, "Photo- and electrical-responsive liquid crystal smart dimmer for augmented reality displays," Opt. Express **27**(13), 18169 (2019).
17. H. H. Khaligh, K. Liew, Y. Han, N. M. Abukhdeir, and I. A. Goldthorpe, "Silver nanowire transparent electrodes for liquid crystal-based smart windows," Sol. Energy Mater. Sol. Cells **132**, 337–341 (2015).

18. S. W. Oh, S. H. Kim, J. M. Baek, and T. H. Yoon, "Optical and thermal switching of liquid crystals for self-shading windows," Adv. Sustainable Syst. **2**(5), 1700164 (2018).

19. M. Bosch, M. R. Shcherbakov, K. Won, H. S. Lee, Y. Kim, and G. Shvets, "Electrically actuated varifocal lens based on liquid-crystal-embedded dielectric metasurfaces," Nano Lett. **21**(9), 3849–3856 (2021).

20. F. Gou, F. Peng, Q. Ru, Y.-H. Lee, H. Chen, Z. He, T. Zhan, K. L. Vodopyanov, and S.-T. Wu, "Mid-wave infrared beam steering based on high-efficiency liquid crystal diffractive waveplates," Opt. Express **25**(19), 22404 (2017).

21. J. Kobashi, H. Yoshida, and M. Ozaki, "Planar optics with patterned chiral liquid crystals," Nat. Photonics **10**(6), 389–392 (2016).

22. H. Yoshida and J. Kobashi, "Flat optics with cholesteric and blue phase liquid crystals," Liq. Cryst. **43**(13-15), 1909–1919 (2016).

23. N. Behabtu, J. R. Lomeda, M. J. Green, A. L. Higginbotham, A. Sinitskii, D. V. Kosynkin, D. Tsentalovich, A. N. G. Parra-Vasquez, J. Schmidt, E. Kesselman, Y. Cohen, Y. Talmon, J. M. Tour, and M. Pasquali, "Spontaneous high-concentration dispersions and liquid crystals of graphene," Nat. Nanotechnol. **5**(6), 406–411 (2010).

24. R. K. Gupta and A. A. Sudhakar, "Perylene-based liquid crystals as materials for organic electronics applications," Langmuir **35**(7), 2455–2479 (2019).

25. Y. Liu, Z. Xu, W. Gao, Z. Cheng, and C. Gao, "Graphene and other 2d colloids: Liquid crystals and macroscopic fibers," Adv. Mater. **29**, 1606794 (2017).

26. X. W. Lin, J. B. Wu, W. Hu, Z. G. Zheng, Z. J. Wu, G. Zhu, F. Xu, B. B. Jin, and Y. Q. Lu, "Self-polarizing terahertz liquid crystal phase shifter," AIP Adv. **1**(3), 032133 (2011).

27. H. Y. Wu, C. F. Hsieh, T. T. Tang, R. P. Pan, and C. L. Pan, "Electrically tunable room-temperature 2π liquid crystal terahertz phase shifter," IEEE Photonics Technol. Lett. **18**(14), 1488–1490 (2006).

28. C. W. Chen, Y. C. Lin, C. H. Chang, P. Yu, J. M. Shieh, and C. L. Pan, "Frequency-dependent complex conductivities and dielectric responses of indium tin oxide thin films from the visible to the far-infrared," IEEE J. Quantum Electron. **46**(12), 1746–1754 (2010).

29. O. Buchnev, J. Wallauer, M. Walther, M. Kaczmarek, N. I. Zheludev, and V. A. Fedotov, "Controlling intensity and phase of terahertz radiation with an optically thin liquid crystal-loaded metamaterial," Appl. Phys. Lett. **103**(14), 141904 (2013).

30. F. Fan, H. J. Zhao, Y. Y. Ji, S. L. Jiang, Z. Y. Tan, J. R. Cheng, and S. J. Chang, "Spin-decoupled beam steering with active optical chirality based on terahertz liquid crystal chiral metadevice," Adv. Mater. Interfaces **10**(7), 2202103 (2023).

31. H.-J. Zhao, F. Fan, Y.-Y. Ji, S.-L. Jiang, Z.-Y. Tan, and S.-J. Chang, "Active terahertz beam manipulation with photonic spin conversion based on a liquid crystal pancharatnam-berry metadevice," Photonics Res. **10**(11), 2658 (2022).

32. H.-J. Zhao, F. Fan, T.-R. Zhang, Y.-Y. Ji, and S.-J. Chang, "Dynamic terahertz anisotropy and chirality enhancement in liquid-crystal anisotropic dielectric metasurfaces," Photonics Res. **10**(4), 1097 (2022).

33. Y. Ji, F. Fan, Z. Zhang, J. Cheng, and S. Chang, "Active terahertz liquid crystal device with carbon nanotube film as both alignment layer and transparent electrodes," Carbon **190**, 376–383 (2022).

34. R. Wang, L. Li, J. Liu, F. Yan, F. Tian, H. Tian, J. Zhang, and W. Sun, "Triple-band tunable perfect terahertz metamaterial absorber with liquid crystal," Opt. Express **25**(26), 32280 (2017).

35. N. Chikhi, M. Lisitskiy, G. Papari, V. Tkachenko, and A. Andreone, "A hybrid tunable thz metadevice using a high birefringence liquid crystal," Sci. Rep. **6**(1), 34536 (2016).

36. L. Yang, F. Fan, M. Chen, X. Zhang, and S. J. Chang, "Active terahertz metamaterials based on liquid-crystal induced transparency and absorption," Opt. Commun. **382**, 42–48 (2017).

37. X. Li, N. Tan, M. Pivnenko, J. Sibik, J. A. Zeitler, and D. Chu, "High-birefringence nematic liquid crystal for broadband thz applications," Liq. Cryst. **43**(7), 955–962 (2016).

38. J. Wang, H. Tian, Y. Wang, X. Li, Y. Cao, L. Li, J. Liu, and Z. Zhou, "Liquid crystal terahertz modulator with plasmon-induced transparency metamaterial," Opt. Express **26**(5), 5769 (2018).

39. J. Yang, P. Wang, T. Shi, S. Gao, H. Lu, Z. Yin, W. Lai, and G. Deng, "Electrically tunable liquid crystal terahertz device based on double-layer plasmonic metamaterial," Opt. Express **27**(19), 27039 (2019).

40. S. Savo, D. Shrekenhamer, and W. J. Padilla, "Liquid crystal metamaterial absorber spatial light modulator for thz applications," Adv. Opt. Mater. **2**(3), 275–279 (2014).

41. Q. Zhao, L. Kang, B. Du, B. Li, J. Zhou, H. Tang, X. Liang, and B. Zhang, "Electrically tunable negative permeability metamaterials based on nematic liquid crystals," Appl. Phys. Lett. **90**(1), 011112 (2007).

42. E. Perivolari, V. A. Fedotov, J. Parka, M. Kaczmarek, and V. Apostolopoulos, "Anomalous resonance frequency shift in liquid crystal-loaded thz metamaterials," Nanophotonics **11**(10), 2341–2348 (2022).

43. M. Oh-E and K. Kondo, "The in-plane switching of homogeneously aligned nematic liquid crystals," Liq. Cryst. **22**(4), 379–390 (1997).

44. R. A. Soref, "Field effects in nematic liquid crystals obtained with interdigital electrodes," J. Appl. Phys. **45**(12), 5466–5468 (1974).

45. M. Oh-E and K. Kondo, "Electro-optical characteristics and switching behavior of the in-plane switching mode," Appl. Phys. Lett. **67**(26), 3895–3897 (1995).

46. U. Chodorow, J. Parka, K. Garbat, N. Paka, and K. Czuprynski, "Spectral investigation of nematic liquid crystals with high optical anisotropy at thz frequency range," Phase Transitions **85**(4), 337–344 (2012).

47. P. U. Jepsen, R. H. Jacobsen, and S. R. Keiding, "Generation and detection of terahertz pulses from biased semiconductor antennas," J. Opt. Soc. Am. B **13**(11), 2424–2436 (1996).

48. P. Dean, A. Valavanis, J. Keeley, K. Bertling, Y. L. Lim, R. Alhathlool, A. D. Burnett, L. H. Li, S. P. Khanna, D. Indjin, T. Taimre, A. D. Rakic, E. H. Linfield, and A. G. Davies, "Terahertz imaging using quantum cascade lasers - a review of systems and applications," J. Phys. D: Appl. Phys. **47**(37), 374008 (2014).

49. B. Beddoes, E. Perivolari, M. Kaczmarek, V. Apostolopoulos, and V. Fedotov, " Dataset for all-optical switching of liquid crystals at terahertz frequencies enabled by metamaterials,", University of Southampton Repository, 15 May 2023, https://doi.org/10.5258/SOTON/D2570.